Lin et al. Nanoscale Research Letters (2018) 13:243
https://doi.org/10.1186/s11671-018-2663-6

Nanoscale Research Letters

NANO EXPRESS Open Access

Strain-Controlled Recombination in InGaN/GaN Multiple Quantum Wells on Silicon Substrates

Tao Lin[1], Zhi Yan Zhou[1], Yao Min Huang[1], Kun Yang[1], Bai Jun Zhang[2] and Zhe Chuan Feng[1*]

Abstract

This paper reports the photoluminescence (PL) properties of InGaN/GaN multiple quantum well (MQW) light-emitting diodes grown on silicon substrates which were designed with different tensile stress controlling architecture like periodic Si δ-doping to the n-type GaN layer or inserting InGaN/AlGaN layer for investigating the strain-controlled recombination mechanism in the system. PL results turned out that tensile stress released samples had better PL performances as their external quantum efficiencies increased to 17%, 7 times larger than the one of regular sample. Detail analysis confirmed they had smaller nonradiative recombination rates ((2.5~2.8)×10^{-2} s^{-1} compared to (3.6~4.7)× 10^{-2} s^{-1}), which was associated with the better crystalline quality and absence of dislocations or cracks. Furthermore, their radiative recombination rates were found more stable and were much higher ((5.7~5.8) ×10^{-3} s^{-1} compared to [9~7] ×10^{-4} s^{-1}) at room temperature. This was ascribed to the suppression of shallow localized states on MQW interfaces, leaving the deep radiative localization centers inside InGaN layers dominating the radiative recombination.

Keywords: InGaN/GaN multiple quantum well, Luminescence, Time-resolved photoluminescence, Silicon substrate

Background

InGaN/GaN multiple quantum well (MQW) structures grown on silicon substrates instead on conventional sapphire have attracted growing attentions for their potential applications in low-cost solid-state lighting, panel display, and silicon photonics [1–5]. The critical obstacle in fabricating high-quality GaN film on Si is the thermal expansion mismatch (56%) between GaN and Si, which introduced large tensile stress and cracks to the grown GaN films [6–9]. Furthermore, a Si doped n-type GaN layer beneath MQW layers is necessary for light-emitting diodes (LEDs) or laser diodes (LDs). In these cases, additional tensile stress from Si doping will be brought in. In recent years, efforts have been made to overcome these difficulties via using intermediate layers with suitable compressive stress to counterbalance tensile stress [10–16], delta doping for strain relaxation [17, 18], or the lattice-matched buffer layer deposition [19, 20]. According to previous works [17], periodic Si δ-doping architecture of the n-type GaN layer could achieve smoother GaN layer with higher crystalline quality and lower crack density than on Si uniformly doped GaN. This was attributed to the reduction of tensile stress. Several works have been done for examining the surface morphology, dislocation density, and electrical properties of crystalline GaN/Si δ-doping GaN layers on either sapphire [21, 22] or silicon substrates [23]. Unfortunately, few of them directly investigated the luminescence properties of InGaN/GaN MQW structures on top of a Si δ-doping GaN layer and clarified the relationship between luminescence efficiency enhancement and strain release caused by the film structure improvements, which are critical to the device fabrication. It is also worth mentioning that, direct measuring strain or observing lattice distortions without breaking down the LED samples is difficult. Indirect methods are always applied to evaluate the internal strain. For instance, mechanical pressure was applied to modulate the internal strain, which led to the changes of piezoelectric field inside MQWs as well as the optoelectronic performances of LED devices

* Correspondence: fengzc@gxu.edu.cn
[1]School of Physical Science and Technology, Laboratory of Optoelectronic Materials and Detection Technology, Guangxi Key Laboratory for Relativistic Astrophysics,, Guangxi University, Nanning 530004, China
Full list of author information is available at the end of the article

[24–27]. In any of these cases, luminescence spectra measurements were found indispensable for exanimating the strain-related device performance.

Therefore, in this work, InGaN/GaN MQW LED structures were deposited on crystalline silicon substrates. Either Si uniformly doped GaN or periodic Si δ-doped GaN working as n-type GaN layer was grown for comparison. Furthermore, two more control samples based on Si uniformly doped n-type GaN layers, inserting by a thin layer of AlGaN or InGaN respectively, were also prepared for supporting the analysis of influence of compressive stress or tensile stress to the device performance, as AlGaN has smaller lattice constant than GaN, which will partially release tensile stress on the surface, as well as InGaN inserted layer will aggravate tensile stress on the contrary. Relative photoluminescence (PL) efficiencies and recombination lifetimes (rates) for each sample were extracted from temperature-varied steady-state (SS) PL spectra and time-resolved (TR) PL spectra and then systematically analyzed. The results turned out that tensile stress released samples had better PL performances as both the nonradiative recombination related to structure defects were suppression and radiative recombination are more connected to deep recombination states inside InGaN well layers, which led to radiative recombination that are more stable with temperature.

Methods

As shown in the schematic of Fig. 1, the epitaxial growth of InGaN/GaN MQWs were performed by metal organic chemical vapor deposition which was reported in previous work [17]: 100 nm AlN layer, 660 nm linearly graded AlGaN layer, and 200 nm nominally undoped GaN layer were grown on the Si (111) substrate as the buffer at 1060, 1060, and 1020 °C, respectively. For samples S1, S3, and S4, 1 μm Si uniformly doped GaN layer was deposited on the buffer with the estimated Si atom concentration around 10^{18} cm^{-3}. For samples S3 and S4, 20 nm InGaN inserted layer with In%~10at% or 20 nm AlGaN inserted layer with Al%~20% was deposited after the n-type Si uniformly doped GaN layer. For sample S2, 20 periods of Si δ-doped planes each followed by 50 nm nominally undoped GaN with a total thickness of 1 μm instead of Si uniformly doped GaN layer was grown on the buffer. After those, on each sample of S1–S4, 6 periods of InGaN/GaN QWs were grown at 800 °C, in which indium composition is around 22.0at%. The average well/barrier thickness was estimated as 2.4 nm/10 nm. After that, 220 nm Mg doped p-type GaN layers were grown at 1020 °C. For PL spectra tests, a Zolix-750 PL system with a 10 mW, 377 nm pulsed laser was used as the excitation light resource, and an ANDOR Newton CCD with 0.09 nm resolution was used as the photodetector. In TRPL measurements, the PL decays were recorded by a time-correlated single-photon counting system in 10–300 K.

Results and Discussion

The overview of SSPL properties for each tested MQW sample at 10 K is shown in Fig. 2. As seen in the insert, the original MQW on Si-structured S1 exhibits emission peaks around 500–650 nm with Fabry-Perot oscillation. PL spectra for all four samples have the same character. This phenomenon is commonly observed in GaN-based

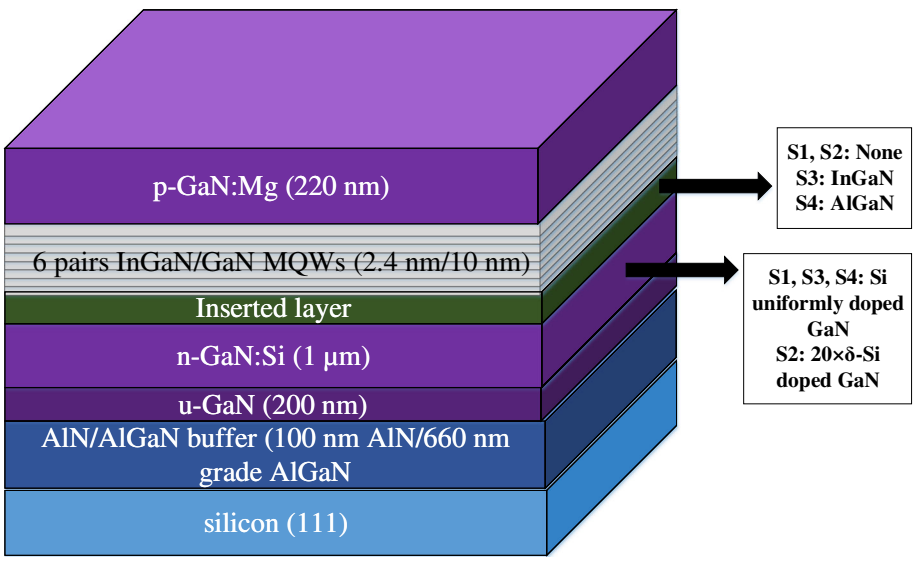

Fig. 1 Structures of the MQW LED samples grown on Si substrates. S1, S3, and S4 contain 1 μm Si uniformly doped n-type GaN layer. S3 contains 20 nm InGaN inserted layer. S4 contains 20 nm AlGaN inserted layer. S2 contains 20 periods of Si-δ-doped planes each followed by 50 nm nominally undoped GaN with a total thickness of 1 μm instead of Si uniformly doped n-type GaN layer

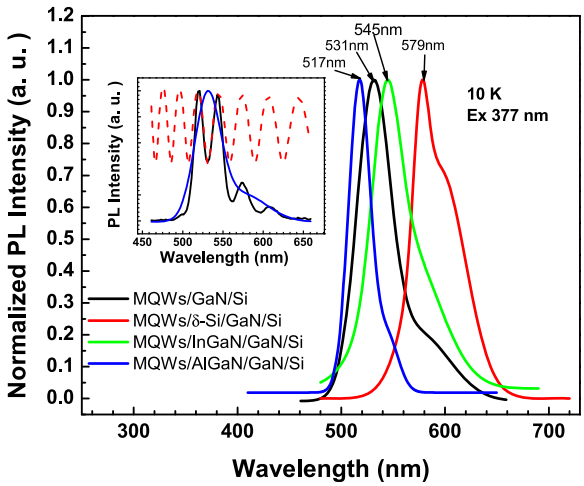

Fig. 2 Overview of SSPL for S1–S4 excited by 377 nm laser at 10 K. The original PL signals contain Fabry-Perot oscillation which is shown as the black curve in the insert (S1 as an example). The oscillation item (red dash curve) and Gaussian PL peak (blue curve) are split by fitting the original signals. All PL data for S1–S4 are treated by the same method, and then, the split Gaussian PL are shown in the figure

LED grown on Si substrates [28–30], as the buffer/Si interface has large reflectance, so a remarkable downward fraction of PL intensity from MQWs is reflected and interferes with the directly upward fraction. These oscillation peaks can be simply described as Gaussian PL signals multiplied by oscillation item (1 + Acos ($4\pi nd/\lambda$)) (demonstrated as the red curve in the insert of Fig. 1), in which A represents the oscillation strength, n is the average refractive index of MQW film, d is the whole thickness of MQW film, and λ is the PL wavelength. According to the above model, the original Gaussian PL peak can be fitted and extracted from the complex oscillation peaks (demonstrated as the blue curve in the insert of Fig. 1). The SSPL result turned out that S1 has a sharp green PL peak at 531 nm, according to the bandgap energy of InGaN crystal with In%~22at%. As comparisons, S2 with Si δ-doped n-type GaN layer has a noteworthily redshifted PL peak at 579 nm, S3 with InGaN inserted layer has a slightly blueshifted PL peak at 517 nm, and S4 with AlGaN inserted layer has a slightly redshifted PL peak at 545 nm. Considering that AlGaN inserted layer plays the role of releasing the tensile stress just familiar with the function of Si δ-doping, whereas InGaN inserted layer aggravates tensile stress, these results indicate that tensile stress on the substrate will lead to the blueshift of MQW PL position or enlargement of the average bandgap of InGaN well. The strain-release effect of Si δ-doped GaN layer is much stronger than that of introduction of inserted layer.

For understanding the recombination nature in MQWs, it is critical to test their PL decay properties because PL lifetimes related to radiative/nonradiative recombination rates can be directly extracted from the decay curves. Here, the PL decays were measured with fixing the detected wavelength at peak values of S1–S4, and the measurements were done at different temperature ranged from 10 to 300 K. Figure 3 shows three typical PL decay curves for S1 tested at 10, 100, and 300 K. It is found that the PL decays for all S1–S4 tend to vary with temperature. This phenomenon reflects the temperature dependences of both radiative recombination rates and nonradiative recombination rates in the samples. Following single exponential decay function was used to fit every decay curve:

$$I(t) = I_0 e^{-t/\tau} \quad (1)$$

where I_0 represents the PL intensity at $t = 0$ and τ represents the PL lifetime. It is worth noted that not all decay curve can be perfectly fitted by above single exponential decay function. This has been widely discussed by several groups [31–34]. A reasonable assumption was that there exist multiple recombination centers in the system. Sometimes multi-exponential decay function was used to fit the curves. Here, to avoid introducing too many assumptions that are hard to be verified at last, or making the analysis incorrectly reflects only on the minor parts of the whole PL properties, we used the simplest model to extract an average PL lifetime for each sample, which may reflect the overall PL dynamic properties. The obtained lifetimes for S1–S4 were put together in Fig. 4a. To connect the PL dynamic results to the recombination probability, recombination rate k was defined as $k = 1/\tau$. Spots of k versus temperature for S1–S4 are also shown in Fig. 4b. The results clearly

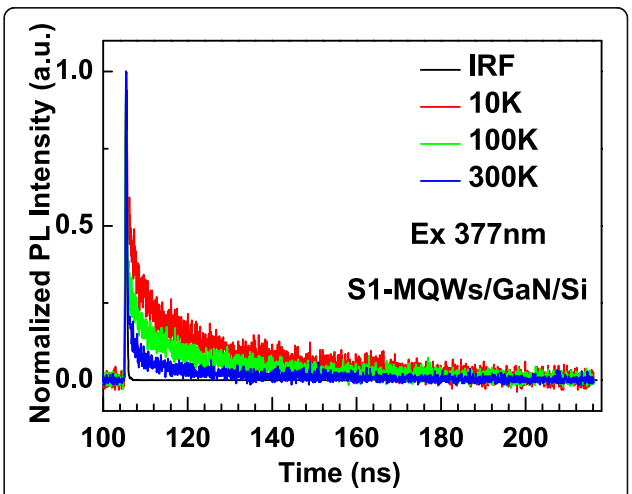

Fig. 3 PL decay curves for S1 excited by 377 nm pulsed laser at 10 K, 100 K, and 300 K

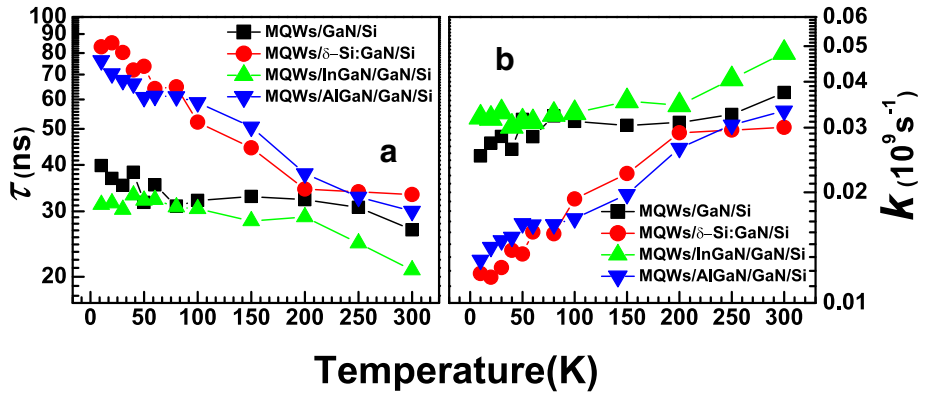

Fig. 4 **a** PL lifetimes vs. temperature for S1–S4. The detected wavelength is kept at each peak position according to SSPL results in Fig. 2. **b** Corresponding recombination rates for S1–S4, which are obtained by $k = 1/\tau$

show two diverse kinds of evolution of k with temperature that the recombination rates for the tensile stress released samples S2 and S4 are smaller than the one for original sample S1 or tensile stress aggravated sample S3 throughout the whole temperature range and increase more severely with increasing temperature. Note that $k = k_r + k_{nr}$, in which k_r represents radiative recombination rate and k_{nr} represents nonradiative recombination rate. It is expected that k_{nr} increases when the temperature rises, and dominates k at room temperature, as it always relates to energy exchange processes with heat [35]. So, the k results at high temperature side in Fig. 4b exhibit the solid evidence that strain release processes such as Si δ-doping and AlGaN inserting have positive influences on suppressing nonradiative recombination in MQWs throughout reducing dislocation defects or cracks that have major influence on k_{nr}. But k_r becomes nonnegligible on low temperature condition. Therefore, additional information and further analysis are needed to explain the behavior of k at low temperature side.

Hence, for splitting k_r and k_{nr} from each k value, SSPL spectra on various temperature condition for each sample were measured. Then, the intensity of each PL peak corresponding to their detected wavelengths on previous TRPL tests were recorded as $I(T)$. After that, relative PL efficiency was defined as $\eta = I(T)/I_0$, in which I_0 represents PL intensity at 0 K. The obtained PL efficiencies for S1–S4 were put together in Fig. 5a. It can be found that the PL efficiencies for S2 and S4 are both around 17%, which are 7 times larger than the one of S1. It is known that only radiative recombination contributes to PL intensity; therefore, this relative PL efficiency reflects the ratio of radiative recombination rate in total recombination rate:

$$\eta = k_r/(k_r + k_{nr}) = k_r/k \tag{2}$$

Thus, it is capable to resolve $k_r = k\eta$ and $k_{nr} = k(1 - \eta)$ from the TRPL results combined with η. The respective calculation for k_r and k_{nr} of S2 was shown in Fig. 5b as

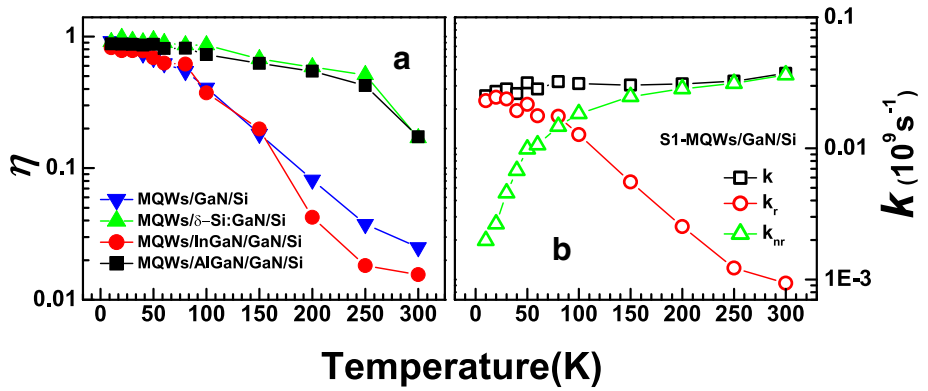

Fig. 5 **a** Relative PL efficiencies vs. temperature for S1–S4. The detected wavelength is kept at each peak position according to SSPL results in Fig. 2. **b** Total recombination rate, radiative recombination rate, and nonradiative recombination rate vs. temperature for S1

an example. The results turned out that even for S2 with Si δ-doping modification, nonradiative recombination rate is larger than radiative recombination rate until reaching a very low temperature of 50 K. This explains the reason why k keeps on increasing when temperature grows because it is dominant in k_{nr}. It also indicates the high demand on further crystalline quality improvement for MQW on Si structures. The radiative recombination rate k_r was found declining monotonously with growing temperature, which does not agree with typical PL properties originating from free electron-hole pair recombination that k_r is free from temperature. However, it is reasonable if the PL process is dominant in exciton localization. Excitons tend to delocalize in higher temperature range; as a result, increasing of temperature will lead to decline of localization rate [32]. k_{nr} and k_r versus temperature for S1–S4 were summarized in Fig. 6a, b, respectively. As shown, the results of k_{nr} at 300 K for S2 and S4 are 2.5×10^{-2} s^{-1} and 2.8×10^{-2} s^{-1}, respectively, which are lower than those for S1 (3.6×10^{-2} s^{-1}) and S4 (4.7×10^{-2} s^{-1}). These further verify that strain release processes suppress the formation of dislocation and cracks in MQWs, consequently decrease the densities of nonradiative recombination centers. This suppression effect becomes more sensitive when temperature goes down. The obtained k_r results are more complicated. As shown, k_r for S1 and S3 decline much more severely than that for S2 and S4 following temperature raise. As a result, obtained k_r at 300 K for S2 (5.7×10^{-3} s^{-1}) and S4 (5.8×10^{-3} s^{-1}) are much higher than that for S1 (9×10^{-4} s^{-1}) and S3 (7×10^{-4} s^{-1}). It is reasonable to ascribe this phenomenon to the strain release processes: according to the above discussion, the radiative processes in these MQW samples are mainly related to exciton recombination in localized states. Here, k_r is mainly determined by exciton localization rate k_{loc}. The dramatical decline of k_{loc} with growing temperature indicates that the average depth of localized states is relatively small in the system, making the exciton easy to delocalize at high temperature. In another word, the average depths of localized states in samples with strain releasing as S1 and S3 are smaller than the ones without strain releasing. Based on the previous works [36], the localized radiative recombination centers in InGaN/GaN MQWs are often offered by structural defects in InGaN well layers, like well thickness variations and indium rich clusters, in which well thickness variations offer shallow states as well as indium rich clusters offer states with much deeper depths [33]. Here, the result of k_r indicates that strong tensile stress on MQW interfaces led by Si substrate and Si-doped GaN may improve the formation of radiative shallow structural defects, so the depth of localized states for S1 and S3 is smaller as well thickness variations are dominant in the exciton localization processes. For S2 and S4, the well thickness variations are suppressed, so the exciton localization processes are dominant in the deep states inside InGaN wells, exhibiting much larger average depths of localized states and more stable k_r versus temperature. Consequently, samples S1 and S3 demonstrate higher k_r than S2 and S4 at low temperature side where exciton delocalization effect is weak, but much smaller k_r at room temperature.

Conclusions

In summary, temperature-varied SSPL and TRPL spectra were studied for different InGaN/GaN MQWs on Si structures with or without tensile stress releasing treatments. It was found that the sample with Si δ-doping GaN layer or AlGaN inserted layer had smaller recombination rate and higher PL efficiency (up to 17%) than the regular sample (2.5%) or sample with InGaN inserted layer (1.6%). Further analysis clarified that the smaller recombination rates were mainly led by smaller dominant nonradiative recombination rates (2.5×10^{-2} s^{-1} for δ-doping sample, 3.6×10^{-2} s^{-1} for AlGaN inserted sample compared to 3.6×10^{-2} s^{-1} for regular sample and 4.7×10^{-2} s^{-1} for InGaN inserted sample), which were

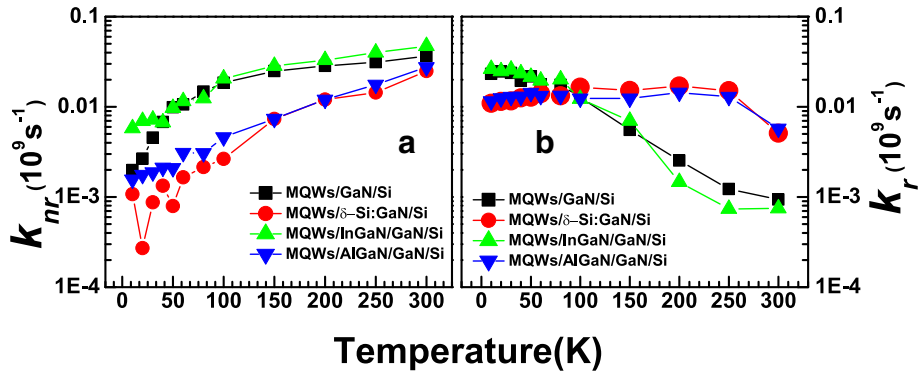

Fig. 6 a Nonradiative recombination rates vs. temperature for S1–S4. **b** Radiative recombination rates vs. temperature for S1–S4

ascribable to the suppression to the formation of dislocations or cracks. Besides smaller nonradiative recombination rates, the better PL performances were also led by the radiative recombination rates that were more stable and higher at room temperature (5.7×10^{-3} s^{-1} for δ-doping sample, 5.8×10^{-3} s^{-1} for AlGaN inserted sample compared to 9×10^{-4} s^{-1} for regular sample and 7×10^{-4} s^{-1} for InGaN inserted sample). They were also ascribable to the suppression of well thickness variations on MQW interfaces, leaving the deep radiative localization centers inside InGaN layers dominate the radiative recombination process. The above results showed a clear picture to the recombination processes of InGaN/GaN MQW LED devices on silicon substrates, which may guide the device fabrication in the future.

Abbreviations

IQE: Internal quantum efficiency; LD: Laser diode; LED: Light-emitting diode; MQW: Multiple quantum well; PL: Photoluminescence; SSPL: Steady-state photoluminescence; TRPL: Time-resolved photoluminescence

Funding

This work is supported by NSFC (61504030, 11533003, and U1731239), Guangxi Natural Science Foundation (2015GXNSFCA139007) and Special Funding for Guangxi Distinguished Professors (Bagui Rencai and Bagui Xuezhe).

Availability of Data and Materials

The datasets used and/or analyzed during the current study are available from the corresponding author on reasonable request.

Authors' Contributions

TL conceived and designed the work. TL and ZF wrote and revised the paper. BZ prepared the samples. ZZ, YH, and KY measured the PL spectra. ZF supervised the research work. All authors read and approved the final manuscript.

Competing Interests

The authors declare that they have no competing interests.

Publisher's Note

Author details

[1]School of Physical Science and Technology, Laboratory of Optoelectronic Materials and Detection Technology, Guangxi Key Laboratory for Relativistic Astrophysics,, Guangxi University, Nanning 530004, China. [2]School of Electronics and Information Technology, State Key Laboratory of Optoelectronic Materials and Technologies, Sun Yat-Sen University, Guangzhou 510275, China.

Received: 19 December 2017 Accepted: 9 August 2018
Published online: 22 August 2018

References

1. Sun Y, Zhou K, Sun Q, Liu J, Feng M, Li Z et al (2016) Room-temperature continuous-wave electrically injected InGaN-based laser directly grown on Si. Nat Photon 10(9):595–599
2. Cai W, Yang Y, Gao X, Yuan J, Yuan W, Zhu H et al (2016) On-chip integration of suspended InGaN/GaN multiple-quantum-well devices with versatile functionalities. Opt Express 24(6):6004–6010
3. Athanasiou M, Smith RM, Pugh J, Gong Y, Cryan MJ, Wang T (2017) Monolithically multi-color lasing from an InGaN microdisk on a Si substrate. Sci Rep 7(1):10086
4. Liao Q, Yang Y, Chen W, Han X, Chen J, Luo H et al (2016) Fabrication and properties of thin-film InGaN/GaN multiple quantum well light-emitting diodes transferred from Si (1 1 1) substrate onto a thin epoxy resin carrier. J Disp Technol 12(12):1602–1608
5. Zhang XW, Lin T, Zhang P, Song HC, Jin H, Xu J et al (2018) Tunable quantum dot arrays as efficient sensitizers for enhanced near-infrared electroluminescence of erbium ions. Nanoscale 10(8):4138–4146
6. Dadgar A, Christen J, Riemann T, Richter S, Bläsing J, Diez A et al (2001) Bright blue electroluminescence from an InGaN/GaN multiquantum-well diode on Si (111): impact of an AlGaN/GaN multilayer. Appl Phys Lett 78(15):2211–2213
7. Egawa T, Moku T, Ishikawa H, Ohtsuka K, Jimbo T (2002) Improved characteristics of blue and green InGaN-based light-emitting diodes on Si grown by metalorganic chemical vapor deposition. Jpn J Appl Phys 41(6B):L663
8. Tawfik WZ, Hyun GY, Ryu S-W, Ha JS, Lee JK (2016) Piezoelectric field in highly stressed GaN-based LED on Si (111) substrate. Opt Mater 55(Supplement C):17–21
9. Lee KJ, Chun J, Kim S-J, Oh S, Ha C-S, Park J-W et al (2016) Enhanced optical output power of InGaN/GaN light-emitting diodes grown on a silicon (111) substrate with a nanoporous GaN layer. Opt Express 24(5):4391–4398
10. Raghavan S, Weng X, Dickey E, Redwing JM (2005) Effect of AlN interlayers on growth stress in GaN layers deposited on (111) Si. Appl Phys Lett 87(14):142101
11. Kim M-H, Do Y-G, Kang HC, Noh DY, Park S-J (2001) Effects of step-graded AlxGa1−xN interlayer on properties of GaN grown on Si (111) using ultrahigh vacuum chemical vapor deposition. Appl Phys Lett 79(17):2713–2715
12. Feltin E, Beaumont B, Laügt M, De Mierry P, Vennéguès P, Lahrèche H et al (2001) Stress control in GaN grown on silicon (111) by metalorganic vapor phase epitaxy. Appl Phys Lett 79(20):3230–3232
13. Xiang P, Liu M, Yang Y, Chen W, He Z, Leung KK et al (2013) Improving the quality of GaN on Si (111) substrate with a medium-temperature/high-temperature bilayer AlN buffer. Jpn J Appl Phys 52(8S):08JB18
14. Wang H-C, Chen M-C, Lin Y-S, Lu M-Y, Lin K-I, Cheng Y-C (2017) Optimal silicon doping layers of quantum barriers in the growth sequence forming soft confinement potential of eight-period In0.2Ga0.8N/GaN quantum wells of blue LEDs. Nanoscale Res Lett 12(1):591
15. Uesugi K, Hikosaka T, Ono H, Sakano T, Nunoue S (2017) Reduction of basal plane defects in (11–22) semipolar InGaN/GaN MQWs fabricated on patterned (113) Si substrates by introducing AlGaN barrier layers. Phys Status Solidi A 214(8):1600823
16. Chen M-C, Cheng Y-C, Huang C-Y, Wang H-C, Lin K-I, Yang Z-P (2016) The action of silicon doping in the first two to five barriers of eight periods In0.2Ga0.8N/GaN multiple quantum wells of blue LEDs. J Lumin 177(Supplement C):59–64
17. Xiang P, Yang Y, Liu M, Chen W, Han X, Lin Y et al (2014) Influences of periodic Si delta-doping on the characteristics of n-GaN grown on Si (111) substrate. J Cryst Growth 387(Supplement C):106–110
18. Markurt T, Lymperakis L, Neugebauer J, Drechsel P, Stauss P, Schulz T et al (2013) Blocking growth by an electrically active subsurface layer: the effect of Si as an antisurfactant in the growth of GaN. Phys Rev Lett 110(3):036103
19. Cheng C-H, Tzou A-J, Chang J-H, Chi Y-C, Lin Y-H, Shih M-H et al (2016) Growing GaN LEDs on amorphous SiC buffer with variable C/Si compositions. Sci Rep 6:19757
20. Cheng C-H, Huang T-W, Wu C-L, Chen MK, Chu CH, Wu Y-R et al (2017) Transferring the bendable substrateless GaN LED grown on a thin C-rich SiC buffer layer to flexible dielectric and metallic plates. J Mater Chem C 5(3):607–617
21. Zheng Z, Chen Z, Chen Y, Huang S, Fan B, Xian Y et al (2012) Analysis and modeling of the experimentally observed anomalous mobility properties of periodically Si-delta-doped GaN layers. Appl Phys Lett 100(21):212102
22. Zhao GY, Adachi M, Ishikawa H, Egawa T, Umeno M, Jimbo T (2000) Growth of Si delta-doped GaN by metalorganic chemical-vapor deposition. Appl Phys Lett 77(14):2195–2197
23. Wang LS, Zang KY, Tripathy S, Chua SJ (2004) Effects of periodic delta-doping on the properties of GaN:Si films grown on Si (111) substrates. Appl Phys Lett 85(24):5881–5883
24. Du C, Jing L, Jiang C, Liu T, Pu X, Sun J et al (2018) An effective approach to alleviating the thermal effect in microstripe array-LEDs via the piezo-phototronic effect. Mater Horiz 5(1):116–122
25. Huang X, Jiang C, Du C, Jing L, Liu M, Hu W et al (2016) Enhanced luminescence performance of quantum wells by coupling piezo-phototronic with plasmonic effects. ACS Nano 10(12):11420–11427
26. Peng M, Li Z, Liu C, Zheng Q, Shi X, Song M et al (2015) High-resolution dynamic pressure sensor array based on piezo-phototronic effect tuned photoluminescence imaging. ACS Nano 9(3):3143–3150

27. Peng M, Zhang Y, Liu Y, Song M, Zhai J, Wang ZL (2014) Magnetic-mechanical-electrical-optical coupling effects in GaN-based LED/rare-earth terfenol-D structures. Adv Mater 26(39):6767–6772
28. Hums C, Finger T, Hempel T, Christen J, Dadgar A, Hoffmann A et al (2007) Fabry-Perot effects in InGaN/GaN heterostructures on Si-substrate. J Appl Phys 101(3):033113
29. Ben Sedrine N, Esteves TC, Rodrigues J, Rino L, Correia MR, Sequeira MC et al (2015) Photoluminescence studies of a perceived white light emission from a monolithic InGaN/GaN quantum well structure. Sci Rep 5:13739
30. Tian P, McKendry JJD, Gong Z, Zhang S, Watson S, Zhu D et al (2014) Characteristics and applications of micro-pixelated GaN-based light emitting diodes on Si substrates. J Appl Phys 115(3):033112
31. Minsky MS, Watanabe S, Yamada N (2002) Radiative and nonradiative lifetimes in GaInN/GaN multiquantum wells. J Appl Phys 91(8):5176–5181
32. Chichibu S, Onuma T, Sota T, DenBaars SP, Nakamura S, Kitamura T et al (2003) Influence of InN mole fraction on the recombination processes of localized excitons in strained cubic InxGa1-xN/GaN multiple quantum wells. J Appl Phys 93(4):2051–2054
33. Liu L, Wang L, Liu N, Yang W, Li D, Chen W et al (2012) Investigation of the light emission properties and carrier dynamics in dual-wavelength InGaN/GaN multiple-quantum well light emitting diodes. J Appl Phys 112(8):083101
34. Lin T, Qiu ZR, Yang J-R, Ding LW, Gao Y, Feng ZC (2016) Investigation of photoluminescence dynamics in InGaN/GaN multiple quantum wells. Mater Lett 173:170–173
35. Zhang X, Chen R, Wang P, Shu J, Zhang H, Song H et al (2018) A soft chemistry-based route to enhanced photoluminescence of terbium ions and tin oxide nanocrystals codoped silica thin films. Appl Surf Sci 452:96–101
36. Lin T, Kuo HC, Jiang XD, Feng ZC (2017) Recombination pathways in green InGaN/GaN multiple quantum wells. Nanoscale Res Lett 12(1):137